http://dx.doi.org/10.5935/0103-5053.20140284

J. Braz. Chem. Soc., Vol. 26, No. 2, 331-337, 2015.
Printed in Brazil - ©2015 Sociedade Brasileira de Química
0103 - 5053 $6.00+0.00

Article

Electrochemical and Optical Investigation of Conductive Polymer and MWCNT Nanocomposite Film

Ali Ehsani,[a] Ferydon Babaei[b] and Hossein Mostaanzadeh[a]*

[a]*Department of Chemistry and* [b]*Department of Physics, Faculty of Science, University of Qom, 3716146611 Qom, Iran*

Composites of multi-walled carbon nanotubes (MWCNT) and conductive polymer with good uniformity were prepared by electropolymerization. Molecular modeling calculations were carried out for electroactive monomer (OAP) polymerization with density functional theory (DFT) level using 6-311G(d,p) basis set for all atoms and Gaussian 03 program package. The reflectance and transmittance amplitudes of the composite were obtained, using the continuity of the tangential components of electrical and magnetic fields at interfaces and solving the algebraic matrix equation. The calculated absorbance spectra as a function of wavelength for MWCNTs dispersed in the conductive polymer are depicted. Band gap of the *p*-type semiconducting film was obtained from the plot of $(\alpha h\nu)^2$ *vs.* photon energy.

Keywords: conductive polymer, composite, CNTs, band gap, absorbance, DFT

Introduction

Carbon nanotubes (CNTs) have a novel structure, a narrow distribution size, highly accessible surface area, low resistivity, and high stability.[1] It has been shown experimentally that the introduction of CNTs into a polymer matrix improves the electric conductivity as well as the mechanical properties of the original polymer matrix.[2-4] Composites of CNT and polypyrrole were also prepared to enhance its electrochemical capacitance performance.[5] The high surface area and conductivity of CNTs may improve the redox properties of conducting polymers. It has been found that carbon nanotube and polyaniline (PANI) composites with good uniformity can be formed by the polymerization of aniline containing well-dissolved single-walled carbon nanotubes (SWCNT).[6,7] The CNT in the composites adhere strongly to the PANI matrix by the formation of a charge-transfer complex rather than the weak van deer Waals interactions between them, which improves dispersion of SWCNTs into the PANI matrix, and results in enhanced electric conductivity. CNTs have been aligned through different techniques, such as template-directed fabrication, template-free chemical vapor deposition, self-assembly, mechanical stretching and electrophoresis, etc.[8-12] However, CNTs introduced into a polymeric matrix disperse randomly, they lose their orientations. Because of the unique one-dimensional structure of nanotubes, a high anisotropy is expected for nanotube-polymer composites. Hence, fabrication of high-performance nanotube-based composites should take into consideration the alignment of CNTs in a certain direction. Melt[13] or electrical spinning of a composite through a narrow hole leads to nanotube alignment, but the method provides only fibers. Aminophenols are interesting members of the class of substituted anilines. The hydroxyl group in the phenyl ring can be oxidized to quinine and quinine can be reduced again. Poly *ortho* aminophenol (POAP) gives a surface film of interesting electrochemical and electrochromic properties when it is electropolymerised in acidic solution.[14-19] Herein, we describe a simple strategy for the aligning of disordered CNT within the conducting polymer matrix by *in situ* electropolymerization using an ionic surfactant as the supporting electrolyte. The CNTs were first dispersed in an aqueous solution containing an ionic surfactant similar to the procedure reported by Islam *et al.*[20] Then, electroactive monomer (OAP) was added into the above mixture and finally electrochemical reaction was preceded at the surface of the glassy carbon (GC) electrode.

In the present work, MWCNT/POAP composite was synthesized by normal pulse voltammetry (NPV) methods and electrochemical properties of the films were investigated by using electrochemical techniques. Optical properties of the composite was obtained using optical modeling.

*e-mail: ehsani46847@yahoo.com, a.ehsani@qom.ac.ir

Experimental

The chemicals used in this work were of Merck origin and were used without further purification. Typical MWCNT were uniform with (Carbon purity: 95%, number of wall: 3-15, outer diameter: 5-20 nm, inner diameter: 2-6 nm, length: 1-10 μm, apparent density: 0.15-0.35 g cm^{-3}, loose agglomerate size: 0.1-3 mm) were used. Their hollow cores and multi-layer walls could be clearly seen by transmission electron microscopy (TEM) observation.[21] All electrochemical measurements were carried out in a conventional three electrodes cell, powered by a potentiostato/galvanostat (EG&G273A) and a frequency response analyzer (EG&G, 1025). The frequency ranges of 100 kHz to 100 mHz and modulation amplitude of 5 mV were employed for impedance studies. POAP films electrodeposited on a GC disk were employed as working electrode. Saturated calomel electrode (SCE) and a platinum wire were used as reference and counter electrodes, respectively. MWCNT/POAP composites were prepared by NPV with 5 mV potential increment and pulse width 0.005 s in a stirring solution containing 0.01 mol L^{-1} monomer, 0.5 mol L^{-1} $HClO_4$, 0.1 mol L^{-1} $LiClO_4$, 5.0×10^{-3} mol L^{-1} sodium dodecyl sulfate (SDS) and 8 wt.% of MWCNT in suspension. SDS was used as an additive in order to suspend MWCNT particles and improve the stability and electroactivity of the resulting films. The effect of SDS on the electropolymerisation of conducting polymer in aqueous solutions was investigated.[16] The thickness of the deposited film on graphite was estimated (85 nm) from the charge consumed in reducing the polymer (Q) and the molar concentration of electro-active sites in the film, which is obtained by the faraday law.[22] TEM was performed using a CEM 902A ZEISS transmission electron microscope, with an accelerating voltage of 80 kV.

Theoretical calculations were carried out at DFT level using the 6-311G(d,p) basis set for all atoms with Gaussian 03 program package. The electronic properties such as highest occupied molecular orbital (HOMO) energy, lowest unoccupied molecular orbital (LUMO) energy and frontier molecular orbital coefficients have been calculated. The molecular sketches of all compound were drawn using Gauss View 03.[23] The natural bond orbital (NBO) analysis suggested by Reed *et al.*[24,25] was applied to determine the atomic charges.

Optical modeling

Considering a region $0 \le z \le d$ occupied by MWCNTs dispersed in the conductive polymer (Figure1).

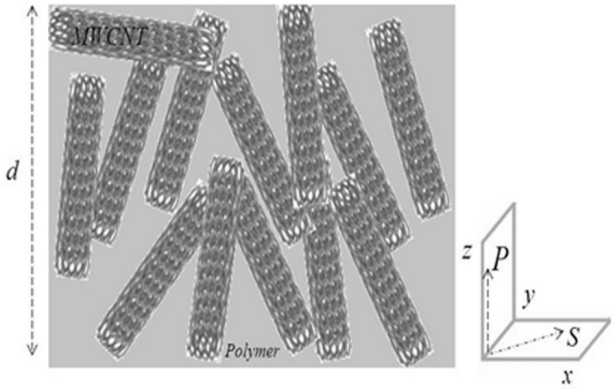

Figure 1. Schematic of the boundary-value problem for optical modeling for MWCNTs dispersed in the conductive polymer.

While the regions $z \le 0$ and $z \ge d$ are vacuous, suppose that an arbitrarily polarized plane wave is normally incident (axial excitation) on the chosen structure from $z \le 0$. The phasors of incident, reflected and transmitted electric fields are given as:

$$\begin{cases} \underline{E}_{inc}(\underline{r}) = [a_s\,\underline{u}_y - a_p\,\underline{u}_x]\,e^{iKz_0}, & z \le 0 \\ \underline{E}_{ref}(\underline{r}) = [r_s\,\underline{u}_y + r_p\,\underline{u}_x]\,e^{-iKz_0}, & z \le 0 \\ \underline{E}_{tr}(\underline{r}) = [t_s\,\underline{u}_y - t_p\,\underline{u}_x]\,e^{iK_0(z-d)}, & z \ge d \end{cases} \quad (1)$$

where (a_s,a_p), (r_s,r_p) and (t_s,t_p) are the amplitudes of incident plane wave, and reflected and transmitted waves with S- or P-polarizations, $K_0 = \omega\sqrt{\mu_0\varepsilon_0} = 2\pi/\lambda_0$ is the free space wave number, λ_0 is the free space wavelength, $\varepsilon_0 = 8.854 \times 10^{-12}\ Fm^{-1}$, $\mu_0 = 4\pi \times 10^{-7}\ Hm^{-1}$ are the permittivity and permeability of free space (vacuum) and $\underline{u}_{x,y,z}$ are the unit vectors in the Cartesian coordinates system. The reflectance and transmittance amplitudes can be obtained using the continuity of the tangential components of electrical and magnetic fields at interfaces and solving the algebraic matrix equation:[26]

$$\begin{bmatrix} t_s \\ t_p \\ 0 \\ 0 \end{bmatrix} = \left[\underline{\underline{K}}\right]^{-1}.\left[\underline{\underline{M}}\right].\left[\underline{\underline{K}}\right].\begin{bmatrix} a_s \\ a_p \\ r_s \\ r_p \end{bmatrix} \quad (2)$$

The different terms and parameters of this equation are given in detail by Lakhtakia.[26] In our work, the absorbance for natural light is defined as $A = -\log[\frac{T_S + T_P}{2}]$, where $T_i = \sum_{j=s,p} T_{ji}$; $T_{i,j} = \left|\frac{t_i}{a_j}\right|^2$; $i, j = s, p$.

Results and Discussion

For phenol derivatives including amino groups, the reported voltammetric studies are interpreted analogously with well-established aniline oxidation, i.e., an E(CE)n mechanism; by which the oxidation of *o*-aminophenol produces a ladder-structured film and reactive intermediates of 2-amino-phenoxazin formation in solution. In order to obtain optimized data concerning polymerization of OAP, theoretical calculations were carried out with DFT. Results are presented in Figure 2 and Tables 1 and 2.

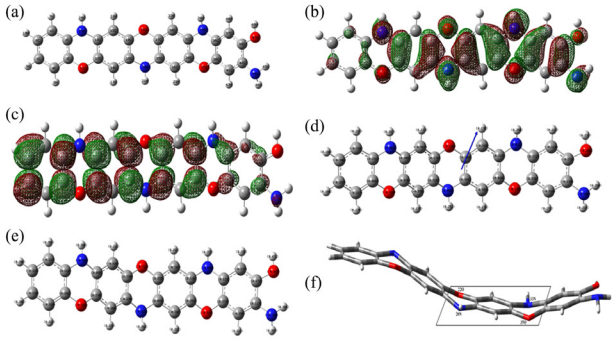

Figure 2. (a) Optimized molecular structure of tetramer; (b) HOMO of tetramer; (c) LUMO of tetramer; (d) Muliken charge population analysis and vector of dipole moment of tetramer; (e) natural charge population analysis of tetramer and (f) schematic representation of the adsorption behavior of tetramer on graphite in acidic solution.

Table1. Orbital energies for HOMO, LUMO, HOMO-LUMO gap energy (ΔE) and dipole moment (μ) of compounds in the gaseous phase[a]

Compound	E_{HOMO} / eV	E_{LUMO} / eV	ΔE / eV	μ / D
tetramer	–4.461	–0.640	4.397	2.5928
trimer	–4.554	–0.594	3.960	1.4926
dimer	–4.774	–0.555	4.219	2.5378
o-aminophenol	–6.203	–0.607	5.596	2.6091

[a]All quantum chemical parameters calculated at DFT level using the 6-311G(d,p) basis set.

The obtained results in Figure 2 and Tables 1 and 2 confirmed that the oxidizing phenol moiety performed the polymerization of the OAP. On the contrary, OAP has a high electronic density in the phenol moiety related to the $–NH_2$ group. Therefore, the preferred pathway is the formation of *p*-quinonimine, which is stabilized by extended conjugation. Therefore, dimers could be formed through attack of the cation radical at that position. The dimer of OAP has the higher electronic density in the *para* position with respect to the –OH group, allowing closing of the phenoxazine ring. The resulting polymer will have a ladder type structure built in by phenozaxine units. Thermodynamic parameters for polymerization of OAP and formation of tetramer have been presented in Table 3. According to obtained results, the dimer and tetramers forms are nearly isoenergetic. Positive values for entropy and energy are related to increasing entropy during oxidation of the monomer and endothermic reaction, respectively. The values of free Gibbs energy are related to applied potential ($\Delta G = -nFE$) during electropolymerisation. The value of calculated potential and applied potential are nearly close together, around 1.16 V. In this case, by applying 1.16 V, oxidation of the monomer leads to the formation of dimer, trimer and tetramer in potentiostatic method.

According to our previous work,[27] TEM has been applied to characterize the electrodeposited nanocomposite film on the surface of the working electrode. Figure 3 shows TEM images of MWCNT/POAP obtained by NPV with potential scale of –0.2 to +0.9 V in an aqueous solution of 0.01 mol L^{-1} monomer, 0.5 mol L^{-1} $HClO_4$, 0.1 mol L^{-1} $LiCO_4$, 5.0×10^{-3} mol L^{-1} SDS and 8% of MWCNT in different magnification surfaces of both the GC electrode and CNT.

These images confirm that MWCNTs have been dispersed in the polymer matrix. From these investigations, it is evident that micelle-encapsulated carbon nanotube composite nanostructures would form by using SDS to disperse carbon nanotubes in aqueous solution,[28,29] and that OAP could enter the interiors of micelle-encapsulated

Table 2. Muliken and natural charges (e) of atoms in tetramer

Atom	11O	22O	35O	47O	23N	20N	33N	44N
Muliken	–0.124	–0.136	–0.139	–0.285	0.003	0.003	0.019	–0.346
Natural	–0.524	–0.727	–0.529	–0.697	–0.596	–0.622	–0.601	–0.796

Table 3. The thermodynamic calculations of some polymerization reactions[a]

Reaction	ΔH° / (kcal mol^{-1})	ΔG° / (kcal mol^{-1})	ΔS° / (cal mol^{-1} K^{-1})
2 a[b] → dimer + 4 H	241.23	225.78	51.82
a + dimer → trimer + 4 H	241.02	224.89	54.10
a + trimer → tetramer + 4 H	241.10	225.01	53.97

[a]All quantum chemical parameters calculated at DFT level using the 6-311G(d,p) basis set; [b]a = *o*-aminophenol.

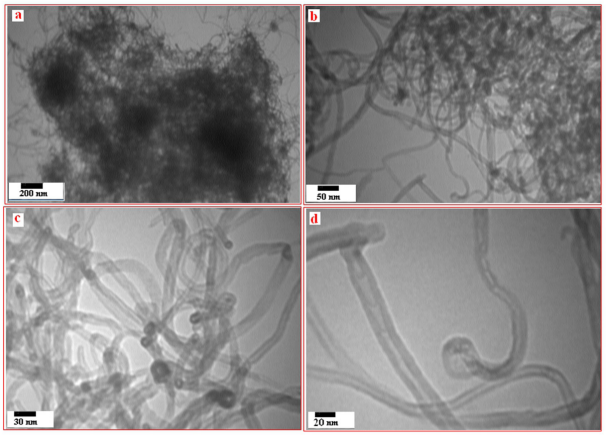

Figure 3. TEM images of MWCNT/POAP in different magnification: (a) scale bare = 200 nm; (b) scale bare = 50 nm; (c) scale bare = 30 nm; (d) scale bare = 20 nm.

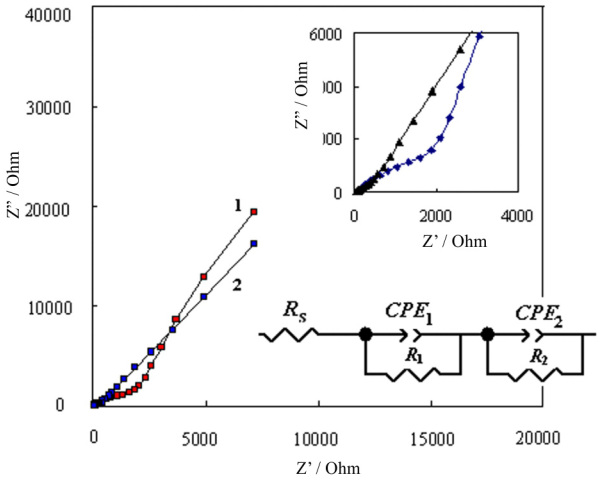

Figure 4. Nyquist diagrams of POAP films in 0.20 V *vs.* SCE in acidic solution, (a) POAP and (b) MWCNT/POAP film. Insets show Nyquist plot in different magnification and equivalent circuit compatible with Nyquist plot.

carbon nanotubes and locate at the interfaces between surfactants and CNT.[20,21] These micelle-encapsulated CNT composite nanostructures had random orientation without an electric field existing. By exerting positive voltage to GC electrode, due to orientation of CNT in the presence of an electric field,[30,31] these micelle-encapsulated CNT composite nanostructures at the vicinities of the GC electrode would orient towards the surface of the GC electrode. Meanwhile, due to the interaction between positive GC electrode and SDS negative ions, the micelle-encapsulated carbon nanotube composite nanostructures would move towards and as far as the surface of the GC electrode. Once micelle encapsulated CNT composite nanostructures ran into the GC electrode, if potentially high enough, OAP located at the interfaces between surfactants and carbon nanotubes would polymerize at the surfaces of both the GC electrode and CNT.

Electrochemical impedance spectroscopy (EIS) is a powerful technique[32-40] used to analyze POAP films in two different synthesis conditions: in acidic solution of $HClO_4$ and $LiClO_4$. Figure 4 shows the Nyquist diagrams of electrodes in 0.2 V dc potential.

The plot in Figure 4 depicts a single semi-circle in the high frequency region and a straight line in the low-frequency region for all spectra. The high-frequency arc is the overall contact impedance generated from the electrical connection between MWCNT/POAP composites and the backing plate as well as the charge transfer at the contact interface between the electrode and the electrolyte solution. In spite of the similar shape of the impedance spectra, there is an obvious difference between the diameters of the semi-circles. That is, the diameters of the semicircles decline greatly with the doping of MWCNT in POAP. In other words, the bulk-film transport of electrons and the charge transfer resistance (R_{ct}) of MWCNT/POAP composite films are much lower than that of the pure POAP films. This means that the MWCNT inside the POAP matrix may lead to a faster electron transport in the bulk-film and charge transfer in the parallel POAP film/solution interface and MWCNT/solution interface, compared to that in the originally single POAP film/solution interface. In conducting polymer/carbon nanotubes composites, it is suggested that either the polymer functionalizes the CNTs,[41] or the conducting polymers are doped with CNTs, i.e., a charge transfer occurs between the two constituents. This fact may suggest that the MWCNT has an obvious improvement effect, which makes the composites have more active sites for faradic reactions and a larger specific capacitance than pure POAP. In addition, this result in enhanced electric conductivity, lowers the resistance and facilitates the charge-transfer of the composites. According to our previous works,[15-19] the behavior of space charge (SC) capacitance *vs.* E (potential) dependence and the observed capacitance values were typical of a thin film semiconductor electrode and suggest the formation of SC or depletion region within the polymer film. This conclusion is consistent with numerous result of another author who demonstrated the formation of a SC region on conducting polymer modified electrodes.[42,43] At the negative potentials, the SC region extends over whole film. As the potential drops across the SC region decrease, its thickness becomes smaller than the film thickness, and a *quasi*-neutral region is formed and the electrode capacitance increases. The dependence of the electrode capacitance on the potential in the simplest case is given by the Mott-Schottky equation:[22]

$$C^{-2} = \frac{2}{\varepsilon\varepsilon_0 eNA^2}\left(E - E_{fb} - \frac{kT}{e}\right) \quad (3)$$

where C is the SC capacitance, ε is the dielectric constant of the polymer, ε_0 is the permittivity of free space, e is the elementary charge, k is Boltzmann's constant, T is the absolute temperature, N is the carrier density that set up the SC, $(E - E_{fb})$ is the absolute value of the potential drop across the SC region. The flat band potential E_{fb} is the potential at which the thickness of the SC region is zero. From equation 3, it follows that C^{-2} *vs.* E line are known as Mott-Schottky plots. Figure 5 presents the C^{-2} *vs.* E dependences for the POAP/MWCNT that obtained from Nyquist plots of films in different offset potential.

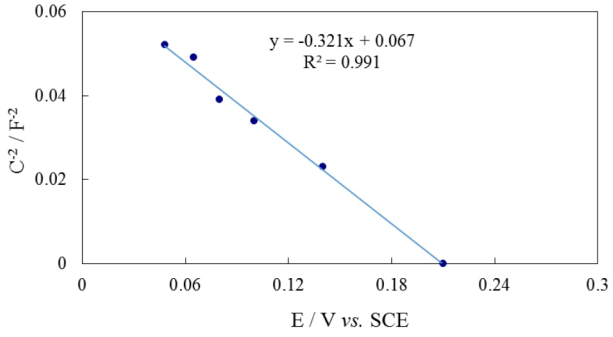

Figure 5. C^{-2} *vs.* E dependences for the MWCNT/POAP composite film.

One can see that each curve has a linear portion that can be described by the Mott-Schottky law to a first approximation. Extrapolating these linear portions, it is possible to estimate the values 0.21 V for the flat band potential of the film. The value of the carrier density can be also obtained 8.98×10^{19} cm^{-3} for the MWCNT/POAP from the slop of the plot. Furthermore, the negative slopes of Mott-Schottky plots show that we can categorize them as *p*-type semiconductors, that SC is established by counter anions.[22,42] In this case, polarons or bipolarons act as holes in ordinary semiconductors.[22]

In optical modeling, the effective dielectric constant for composite medium MWCNT in conductive polymer is obtained as $\varepsilon_{eff} = \varepsilon_2 + \frac{f\varepsilon_2(\varepsilon_1-\varepsilon_2)}{\varepsilon_2 + L(\varepsilon_1-\varepsilon_2) - fL(\varepsilon_1-\varepsilon_2)}$[44-50] using Maxwell-Garnett theory (MGT), where ε_2 and ε_1 are dielectric constant of conductive polymer and MWCNT, while *f* is the volume fraction of MWCNT and L is depolarization factor (for polarizations P = 1/2, S = 0). We have used the birefringence refractive indexes of graphite[43] and bulk conductive polymer for homogenization.[51] Due to birefringence, the dielectric function of graphite consists of two components: ε_0 and ε_e, which correspond to the ordinary and extraordinary rays, respectively. We considered dielectric constant of MWCNT for P and S polarizations as $\varepsilon_1^P = \sqrt{\varepsilon_o \varepsilon_e}$ and $\varepsilon_1^S = \varepsilon_0$. In our work, *f* and d were, respectively, 0.08 and 85 nm, according to experimental results. The calculated absorbance spectra as a function of wavelength for MWCNT dispersed in the conductive polymer are depicted in Figure 6a. The plot of $(\alpha h\nu)^2$ *vs.* photon energy is shown in Figure 6b, where $\alpha = 2.303\frac{A}{d}$; A is absorbance and d is thickness of the film. It has been observed that the photon $(\alpha h\nu)^2$ *versus* $h\nu$ is linear over a wide range of photon energy indicating the direct type of transition. The intercept (extrapolation) of this plot (straight line) on the energy axis give the energy band gap. The direct band gaps E_g was determined as 2.40 eV. The obtained energy is lower than the band gap energy of the polyaniline in the reduced state.[52]

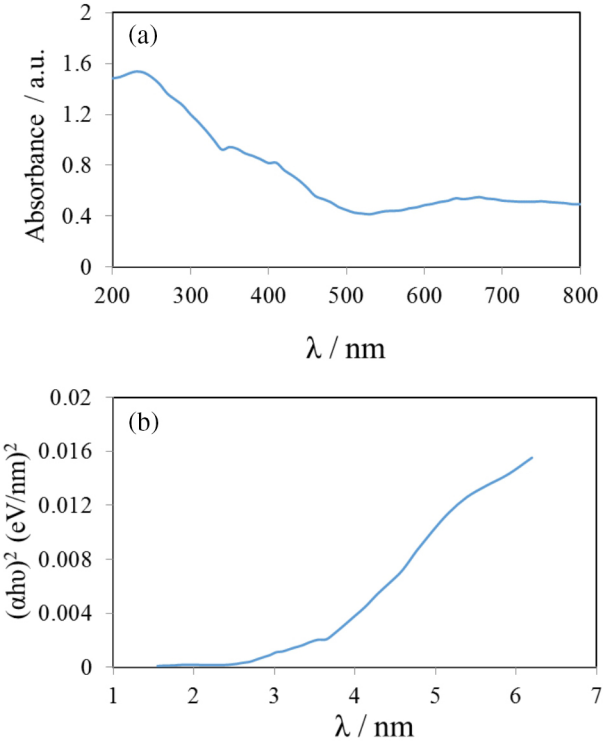

Figure 6. Calculated absorbance and $(\alpha h\nu)^2$ for MWCNT dispersed in the conductive polymer (a) absorbance *vs.* wavelength; (b) $(\alpha h\nu)^2$ *vs.* photon energy.

Conclusions

We have introduced the MWCNT/POAP composite electrode to improve the specific capacitance and power characteristic of electrochemical capacitance. The reflectance and transmittance amplitudes were obtained using the continuity of the tangential components of electrical and magnetic fields at interfaces and solving the algebraic matrix equation. The calculated absorbance spectra as a function of wavelength for MWCNT dispersed in the conductive polymer are depicted. Band gap of the

p-type semiconducting film obtained from the plot of $(\alpha h\nu)^2$ *vs.* photon energy.

Acknowledgements

The authors would like to express their deep gratitude to the Iranian Nano Council for supporting this work.

References

1. Niu, C. M.; Sichel, E. K.; Hoch, R.; Moy, D.; *Appl. Phys. Lett*. **1997**, *70,* 1480.
2. Schadler, L. S.; Giannaris, S. C.; Ajayan, P. M.; *Appl. Phys. Lett*. **1998**, *73,* 3842.
3. Wagner, H. D.; Lourie, O.; Feldman, Y.; Tenne, R.; *Appl. Phys. Lett*. **1998**, *72,* 188.
4. Qian, D.; Dickey, E. C.; Andrews, R.; Rantell, T.; *Appl. Phys. Lett*. **2000**, *76,* 2868.
5. Hughes, M.; Chen, G. Z.; Shaffer, M. S. P.; Fray, D. J.; *Chem. Mater*. **2002**, *14,* 1610.
6. Li, X. H.; Wu, B.; Huang Zhang, J.; Liu, Z. F.; Li, H. L.; *Carbon* **2003**, *41,* 1670.
7. Hosseini, S. M.; Jeddi, F.; Nemati, M.; Madaeni, S. S.; Moghadassi, A. R.; *Desalination* **2014**, *341,* 107.
8. Heer, W. A.; Bonard, J. M.; Fauth, K.; Chatelain, A.; Forro, L.; Ugarte, D.; *Adv. Mater*. **1997**, *9,* 87.
9. Rao, C. N. R.; Sen, R.; Satishkumar, B. C.; Govindaraj, A.; *Chem. Commun*. **1998**, *15,* 1525.
10. Liu, Z.; Shen, Z.; Zhu, T.; Hou, S.; Ying, L.; Shi, Z.; Gu, Z.; *Langmuir* **2000**, *16, 3569*.
11. Ajayan, P. M.; *Adv. Mater*. **1995**, *7,* 489.
12. Yamamoto, K.; Akita, S.; Nakayama, Y.; *J. Appl. Phys*. **1996**, *35,* 917.
13. Haggenmueller, R.; Gommans, H. H.; Rinzler, A. G.; Fischer, J. E.; Winey, I.; *Chem. Phys. Lett*. **2000**, *330,* 219.
14. Ehsani, A.; Babaei, F.; Nasrollahzadeh, M.; *Appl. Surf. Sci.* **2013**, *283,* 1060.
15. Ehsani, A.; Mahjani, M. G.; Bordbar, M.; Adeli, S.; *J. Electroanal. Chem.* **2013**, *710,* 29.
16. Ehsani, A.; Mahjani, M. G.; Jafarian, M.; Naeemy, A.; *Prog. Org. Coat*. **2010**, *69,* 510.
17. Ehsani, A.; Mahjani, M. G.; Jafarian, M.; *Synth. Met*. **2011**, *161,* 1760.
18. Ehsani, A.; Mahjani, M. G.; Jafarian, M.; *Synth. Met*. **2012**, *62,* 199.
19. Ehsani, A.; Mahjani, M. G.; Bordbar, M.; Moshrefi, R.; *Synth. Met*. **2013**, *165,* 51.
20. Islam, M. F.; Rojas, E.; Bergey, D. M.; Johnson, A. T.; Yodh, A. G.; *Nano Lett.* **2003**, *3,* 269.
21. Zhang, X. T.; Zhang, J.; Wang, R. M.; Liu, Z. F.; *Carbon* **2004**, *42,* 1455.
22. Mahjani, M. G.; Ehsani, A.; Jafarian, M.; *Synth. Met*. **2010**, *160,* 1252.
23. Frisch, A. E.; Frisch, M. J.; Trucks, G.; *Gaussian 03 User's Reference*, Gaussian Inc., Pittsburgh, 2003.
24. Reed, A. E.; Weinhold, F.; *Chem. Rev*. **1998**, *88,* 899.
25. Schelegel, H. B.; *Ab Initio Methods in Quantum Chemistry*, John Wiley: New York, 1987.
26. Lakhtakia, A.; Messier, R.; *Sculptured Thin Films, Nano Engineered Morphology and Optics*, SPIE: USA, 2005.
27. Nasrollahzadeh, M.; Azarian, A.; Ehsani, A.; Khalaj, M.; *J. Mol. Catal. A: Chem.* **2014**, *394*, 205.
28. Kang, Y.; Taton, T. A.; *J. Am. Chem. Soc*. **2003**, *125,* 5650.
29. Moore, V. C.; Strano, M. S.; Haroz, E. H.; Hauge, R. H.; *Nano Lett*. **2003**, *3,* 1379.
30. Kumar, M. S.; Kim, T. H.; Lee, S. H.; Song, S. M.; Yang, J. W.; Nahm, K. S.; Suh, E. K.; *Chem. Phys. Lett.* **2004**, *383,* 235.
31. Kumar, M. S.; Kim, T. H.; Lee, S. H.; Song, S. M.; Yang, J. W.; Nahm, K. S.; Suh, E. K.; *J. Solid. State Electr*. **2003**, *47,* 2075.
32. Ehsani, A.; Mahjani, M. G.; Jafarian, M.; *Turk. J. Chem*. **2011**, *35,* 1.
33. Ehsani, A.; Mahjani, M. G.; Jafarian, M.; Naeemy, A.; *Electrochim. Acta* **2012**, *71,* 128.
34. Ehsani, A.; Jaleh, B.; Nasrollahzadeh, M.; *J. Power Sources* **2014**, *257,* 300.
35. Ehsani, A.; Nasrollahzadeh, M.; Mahjani, M. G.; Moshrefi, R.; Mostaanzadeh, H.; *J. Indust. Eng. Chem*. **2014**, *20*, 4363.
36. Ehsani, A.; Adeli, S.; Babaei, F.; Mostaanzadeh, H.; Nasrollahzadeh, M.; *J. Electroanal. Chem*. **2014**, *713,* 91.
37. Nasrollahzadeh, M.; Ehsani, A.; Rostami-Vartouni, A.; *Ultrason. Sonochem.* **2014**, *21,* 275.
38. Ehsani, A.; Mahjani, M. G.; Adeli, S.; Moradkhani, S.; *Prog. Org. Coat*. **2014**, *77,* 1674.
39. Ehsani, A.; Mahjani, M. G.; Nasseri, M.; Jafarian, M.; *Anti-Corros. Methods Mater*. **2014**, *61,* 146.
40. Ehsani, A.; Mahjani, M. G.; Moshrefi, R.; Mostaanzadeh, H.; Shabani- Shayeh, J.; *RSC Adv.* **2014**, *4,* 2003.
41. Baibarac, M.; Baltog, I.; Lefrant, S.; Mevellec, J. Y.; Chauvet, O.; *Chem. Mater*. **2003**, *15,* 4149.
42. Sunde, S.; Hagen, G.; Odegard, R.; *J. Electroanal. Chem*. **1993**, *345*, 59.
43. Bobacka, J.; Grzeszezuk, M.; Ivaska, A.; *Electrochim. Acta* **1992**, *37*, 1759.
44. Lu, W.; Dong, J.; Li, Z. Y.; *Phys. Rev. B: Condens. Matter Mater. Phys.* **2000**, *63*, 033401.
45. Wang, X. J.; Flicker, J. D.; Lee, B. J.; Ready, W. J.; Zhang, Z. M.; *Nanotechnology* **2009**, *20,* 215704.
46. Nasrollahzadeh, M.; Azarian, A.; Ehsani, A.; Khalaj, M.; *J. Mol. Catal. A: Chem.* **2014**, *394,* 205.
47. Nasrollahzadeh, M.; Azarian, A.; Ehsani, A.; Sajadi, S. M.; Babaei, F.; *Mater. Res. Bull*. **2014**, *55,* 168.
48. Nasrollahzadeh, M.; Babaei, F.; Ehsani, A.; Sajadi, S. M.;

Spectrochim. Acta, Part A **2014**, *132,* 423.
49. Nasrollahzadeh, M.; Azarian, A.; Ehsani, A.; Zahraei, A.; *Tetrahedron Lett.* **2014**, *55,* 2813.
50. Palik, E. D.; *Handbook of Optical Constants of Solids*, Academic Press: New York, 1985.
51. Mo, D.; Lin, Y. Y.; Tan, J. H.; Yu, Z. X.; Zhou, G. Z.; Gong, K. C.; Zhang, G. P.; He, X. F.; *Thin Solid Films* **1993***, 234,* 463.
52. Kwon, O.; McKee, M. L.; *J. Phys. Chem. B.* **2000**, *104*, 1686.

Submitted on: July 19, 2014
Published online: December 2, 2014